Spectral analysis of quantum-resonance zones, quantum Kolmogorov-Arnold-Moser theorem, and quantum-resonance overlap

W. A. Lin and L. E. Reichl

Center for Statistical Mechanics, University of Texas, Austin, Texas 78712

The quasienergy spectrum of a particle in an infinite square well perturbed by a monochromatic external field is analyzed in terms of single- and double-resonance Hamiltonians. At small-enough perturbations the quasienergies are accurately given by those obtained from a single-resonance, integrable Hamiltonian. This indicates the existence of a local constant of motion and is a quantum manifestation of the Kolmogorov-Arnold-Moser theorem. At larger perturbations, the quasienergy spacing distributions are Poissonian for the single-resonance Hamiltonian. But for the double-resonance Hamiltonian, the distributions undergo a transition from Poissonian toward Wigner-like behavior when the perturbation is increased from a regime without resonance overlap to a regime with resonance overlap. This indicates the destruction of the local constant of motion through quantum-resonance overlap and its associated quantum number. It is a quantum manifestation of classical-resonance overlap.

I. INTRODUCTION

There is now a large amount of evidence showing that classically integrable and nonintegrable conservative systems have distinct spectral statistics in their corresponding quantum systems.[1-4] Extensive work[5,6] on the distribution of nearest-neighbor spacing of energy levels of nuclei has shown that a pure sequence of levels[5] exhibits level repulsion leading to a Gaussian orthogonal ensemble (GOE) distribution of nearest-neighbor spacings. However, for a mixed sequence,[5] a superposition of pure sequences, the spacing distribution tends to be a Poissonian. Mehta has proved that the spacing distribution of a mixed sequence is a Poisson distribution in the limit when the mixed sequence is composed of an infinite number of pure sequences, whatever the underlying distribution for the pure sequence, based on the assumption that all the pure sequences are uncorrelated (we shall refer to this as Mehta's theorem).[7]

Considering systems with two degrees of freedom, if we study the statistics of a sequence of energy levels without regard to the presence of any quantum numbers, such a sequence would be a mixed sequence for an integrable system. Therefore the resulting spacing distribution tends to be Poissonian. But for a nonintegrable system which is classically chaotic in all parts of phase space (such as the one studied by Bohigas et al. in Ref. 1), the sequence would be a pure sequence which exhibits strong level repulsion leading to a GOE spacing distribution.[1] For a near-integrable system, for which the Kolmogorov-Arnold-Moser (KAM) theorem applies, at small enough perturbations the system behaves like an integrable system in certain parts of phase space, indicating the existence of a local constant of motion. At larger perturbations, such a local constant of motion eventually gets destroyed. Thus, for the corresponding quantum system, one can then use the spacing distribution to determine the existence or absence of a quantum local constant of motion and its corresponding quantum number. Classically, the existence or absence of an additional constant of motion can determine whether or not the underlying dynamics is regular or chaotic. As we shall see, it also has a strong effect on the dynamics of quantum systems.

In addition to the spacing distribution of the spectrum, the Δ_3 statistic of Dyson and Mehta[8] has also been used to study the spectral characteristic. It measures the long-range spectral correlation, while the spacing distribution measures the short-range correlation.

The above techniques can also be applied for time-periodic systems. In this case, we must study its quasienergy spectrum.[9,10] This is because a one-degree-of-freedom time-periodic Hamiltonian system can be viewed as a conservative Hamiltonian system with two degrees of freedom[11] and the quasienergy corresponds to the total energy in this two-degree-of-freedom system.[12]

It is well known that, classically, the destruction of a local constant of motion and onset of global chaos are a result of overlap of resonance zones.[13] A quantum analog to the classical-resonance zones was first shown to exist by Berman et al. for a model which involves two interacting quantum nonlinear resonances.[14] We have shown[15] the existence of external-field-induced quantum-resonance zones for a model describing a particle in an infinite square well driven by a monochromatic external field. Just as for the classical case,[16] these resonance zones overlap when certain parameters of the system are increased to sufficiently large values. In this paper, we will show that there is a change in spacing distribution when quantum-resonance zones overlap, indicating the destruction of a quantum local constant of motion.

Our model consists of a particle in an infinite square-

well potential driven by a monochromatic external force. The classical system has been considered previously,[16] where we showed that an infinite number of resonance zones converge at low energy. As a result, a stochastic layer was found there. The quantum version was subsequently studied.[15] An exactly similar convergence of the quantum-resonance zones was also found at low energy. We will examine the spectral statistics of quantum-resonance zones. We will work in the atomic units where $\hbar = m_e = e = 1$ ($\hbar$ is Planck's constant divided by 2π, m_e is mass of an electron, and e is electron charge). The mass is fixed at that of an electron, $m = 1$. The size of the well is kept at 10 (i.e., 10 Bohr radii). Thus, our parameters are chosen to probe the full quantum domain.

We begin our discussion in Sec. II, with a brief description of our model and its resonance approximations. In Sec. III we make use of the quasienergy-state theory and the properties of the Mathieu equation to extract useful constraints on the allowed quasienergy spectrum for the single-resonance approximation. In Sec. IV we discuss the spectrum we use for statistical analysis and compare the result obtained from the fast-Fourier transform with that predicted in Sec. III for single-resonance approximation. In Sec. V we present the spacing distribution of the quasienergy spectrum when the external field amplitude is just below and above the threshold of overlap of two dominating resonance zones. In Sec. VI we compute the Δ_3 statistic of the spectrum. In Sec. VII some concluding remarks are presented.

II. THE MODEL

We consider the following Hamiltonian for a particle in an infinite square well driven by a monochromatic external field:

$$\hat{H} = \frac{\hat{p}^2}{2m} + \lambda(\hat{x} - a)\cos(\omega_0 t) , \qquad (2.1)$$

where $\hat{p}$ is the momentum operator, m is the mass of the particle, $\hat{x}$ is the position operator, λ is the amplitude of the external field, ω_0 is the angular frequency of the external field, and t is the time. The walls of the well are located at 0 and $2a$. The wave function vanishes at and outside the walls.

In the position representation, the unperturbed energy eigenvector $|n;E\rangle$ takes the following form:

$$\langle x | n;E \rangle = \sqrt{1/a}\,\sin(n\pi x/2a) \quad (n = 1,2,\dots) . \qquad (2.2)$$

The perturbed Hamiltonian can then be expressed as[15]

$$\hat{H} = \sum_{n=1}^{\infty} \hbar\Omega n^2 |n;E\rangle\langle n;E| - \frac{4a\lambda}{\pi^2}\cos(\omega_0 t)$$

$$\times \sum_{N=1;\text{odd}}^{\infty} \sum_{M=1;\text{odd}}^{\infty} \frac{1}{N^2}\left[\left|\frac{M+N}{2}\right\rangle\left\langle\frac{M-N}{2}\right| \right.$$

$$\left. + \left|\frac{M-N}{2}\right\rangle\left\langle\frac{M+N}{2}\right|\right] , \qquad (2.3)$$

with $\langle x | -n;E \rangle = -\langle x | n;E \rangle$. The Schrödinger equation in the representation of the unperturbed energy levels takes the form

$$i\hbar\frac{d\langle n;E | \psi(t)\rangle}{dt}$$

$$= \hbar\Omega n^2\langle n;E | \psi(t)\rangle$$

$$- \frac{4a\lambda}{\pi^2}\cos(\omega_0 t)\sum_{N=1;\text{odd}}^{\infty}\frac{1}{N^2}[\langle n-N;E | \psi(t)\rangle$$

$$+ \langle n+N;E | \psi(t)\rangle] , \qquad (2.4)$$

where $\Omega = \hbar\pi^2/8ma^2$. By introducing the following generating function,

$$\langle \phi | \psi(t)\rangle = \frac{1}{2i\sqrt{\pi}}\sum_{n=-\infty}^{\infty}\frac{e^{in\phi}}{\sqrt{2\pi}}\langle n;E | \psi(t)\rangle , \qquad (2.5)$$

the Schrödinger equation in the angle representation becomes

$$i\hbar\frac{\partial\langle\phi | \psi(t)\rangle}{\partial t}$$

$$= -\hbar\Omega\frac{\partial^2\langle\phi | \psi(t)\rangle}{\partial\phi^2}$$

$$- \frac{4a\lambda}{\pi^2}\sum_{N=1;\text{odd}}^{\infty}\frac{1}{N^2}[\cos(N\phi-\omega_0 t)$$

$$+ \cos(N\phi+\omega_0 t)]\langle\phi | \psi(t)\rangle . \qquad (2.6)$$

The similarity with the classical-resonance zone structure is evident. In fact, if we express the classical Hamiltonian in terms of the canonical variables which are action and angle variables of the unperturbed system (as we did in Ref. 16), then quantize the canonical variables, we immediately obtain the above expression. Alternatively, one can also work in the representation of the unperturbed action. To do this, we introduce the expansion

$$\langle\phi | \psi(t)\rangle = \sum_{j=-\infty}^{\infty}\langle\phi | j;I\rangle\langle j;I | \psi(t)\rangle$$

in Eq. (2.6) and obtain

$$i\hbar\frac{d}{dt}\langle j;I | \psi(t)\rangle$$

$$= n^2\hbar\Omega\langle j;I | \psi(t)\rangle$$

$$- \frac{4a\lambda}{\pi^2}\cos(\omega_0 t)\sum_{N=1;\text{odd}}^{\infty}\frac{1}{N^2}[\langle j-N;I | \psi(t)\rangle$$

$$+ \langle j+N;I | \psi(t)\rangle] , \qquad (2.7)$$

where $|j;I\rangle$ is an eigenstate of the action operator $\hat{I} = -i\hbar\partial/\partial\phi$ and j is an integer. From Eq. (2.5) one can

see that $\langle -\phi \mid \psi(t) \rangle = -\langle \phi \mid \psi(t) \rangle$. This leads to the condition

$$\langle -j;I \mid \psi(t) \rangle = -\langle j;I \mid \psi(t) \rangle \ . \tag{2.8}$$

Each of the cosine traveling potential wells in Eq. (2.6) gives rise to a nonlinear quantum-resonance zone in action space. The centers of the zones are located at $J = \pm \omega_0 / 2N\Omega$.[15] The width of each zone has also been estimated.[15] For small enough λ and high enough ω_0, the resonance zones are well separated.[15] If the initial population [i.e., $\langle j;I \mid \psi(0) \rangle$] for $j > 0$ is nonzero only within or near a given zone, N_0, and far away from any other zone, then one can show,[12] by neglecting terms with fast changing phases in Eq. (2.7), that $\langle j;I \mid \psi(t) \rangle$ for $j > 0$ [the populations for $j < 0$ are always understood to follow the condition $\langle -j;I \mid \psi(t) \rangle = -\langle j;I \mid \psi(t) \rangle$], to a good approximation, is given by $\langle j;I \mid \chi_+^{(0)}(t) \rangle$ for $j > 0$. $\langle j;I \mid \chi_+^{(0)}(t) \rangle$ satisfies the following equation:

$$i\hbar \frac{d}{dt} \langle j;I \mid \chi_+^{(\hbar)}(t) \rangle$$
$$= j^2 \hbar \Omega \langle j;I \mid \chi_+^{(\hbar)}(t) \rangle$$
$$- \sum_{\substack{N=N_0;\text{odd} \\ \hbar \text{ even}}}^{N_0 + \hbar} \frac{2a\lambda}{\pi^2 N^2} [\langle j-N;I \mid \chi_+^{(\hbar)}(t) \rangle e^{-i\omega_0 t}$$
$$+ \langle j+N;I \mid \chi_+^{(\hbar)}(t) \rangle e^{i\omega_0 t}] \tag{2.9}$$

for all integer j, and $\hbar = 0$. In the angle representation Eq. (2.9) can be written as

$$i\hbar \frac{\partial \langle \phi \mid \chi_+^{(\hbar)}(t) \rangle}{\partial t}$$
$$= -\hbar \Omega \frac{\partial^2 \langle \phi \mid \chi_+^{(\hbar)}(t) \rangle}{\partial \phi^2}$$
$$- \sum_{\substack{N=N_0 \text{odd} \\ \hbar \text{ even}}}^{N_0 + \hbar} \frac{4a\lambda}{N^2 \pi^2} \cos(N\phi - \omega_0 t) \langle \phi \mid \chi_+^{(\hbar)}(t) \rangle \ , \tag{2.10}$$

with the condition $\langle \phi + 2\pi \mid \chi_+^{(\hbar)}(t) \rangle = \langle \phi \mid \chi_+^{(\hbar)}(t) \rangle$. For $\hbar = 0$, Eqs. (2.9) and (2.10) describe the behavior of a single isolated nonlinear quantum-resonance zone.

For larger λ, when zones $N = N_0$ and $N = N_0 + 2$ overlap but zones $N = N_0$ and $N = N_0 - 2$ do not, generally all $N > N_0 + 2$ zones will have overlapped with their neighboring zones and they will also be connected with the zones on the negative-j side. The most accurate approximation must then maintain all those terms. Computationally, this is not possible. Fortunately, due to the factor $1/N^2$ in the equations, the dominant contributions come from terms with small N. For the purpose of determining whether an additional constant of motion exists,

it is sufficient to keep only the two largest overlapping zones [take $\hbar = 2$ in Eqs. (2.9) and (2.10)].

III. THE THEORY OF QUASIENERGY STATES

It has been shown previously[15] that the solution to Eq. (2.10) (for $\hbar = 0$) can be found in the rest frame of the traveling cosine potential well by introducing a change of variables:

$$\theta = \tfrac{1}{2}(N_0 \phi - \omega_0 t) \ ,$$
$$T = t \ , \tag{3.1}$$
$$G(\theta, T) = \langle \phi \mid \chi_+^{(0)}(t) \rangle \ .$$

The stationary states in this frame were found to be of the following form:

$$G(\theta, T) = \exp\left[\frac{i\omega_0 \theta}{\Omega N_0^2}\right] \exp\left[\frac{i\omega_0^2 T}{4\Omega N_0^2}\right]$$
$$\times \exp\left[\frac{-i\alpha N_0^2 \Omega T}{4}\right] U_\alpha(\theta) \ , \tag{3.2}$$

where $U_\alpha(\theta)$ satisfies the Mathieu equation

$$\frac{d^2 U_\alpha(\theta)}{d\theta^2} + \alpha U_\alpha(\theta) + 2\rho \cos(2\theta) U_\alpha(\theta) = 0 \ , \tag{3.3}$$

with $\rho = 8a\lambda / \hbar \Omega \pi^2 N_0^4$.

The Hamiltonian leading to Eq. (2.10) is time dependent and has a period of the external field. Therefore we can apply the theory of quasienergy states.[9,10] The most general solution to the Schrödinger equation can be written as

$$\Phi(\phi, t) = \sum_i a_i W_{\varepsilon_i}(\phi, t) e^{-i\varepsilon_i t / \hbar} \ , \tag{3.4}$$

where a_i are constants and $W_{\varepsilon_i}(\phi, t)$ satisfies the following eigenvalue equation:

$$\left[\hat{H}(\phi, t) - i\hbar \frac{\partial}{\partial t}\right] W_{\varepsilon_i}(\phi, t) = \varepsilon_i W_{\varepsilon_i}(\phi, t) \ , \tag{3.5}$$

with $W_{\varepsilon_i}(\phi, t) = W_{\varepsilon_i}(\phi, t + \tau)$, $\tau = 2\pi / \omega_0$. ε_i is called quasienergy.

To find the most general solution to Eq. (2.10) for $\hbar = 0$ we must find the quasienergy states. Using Eq. (3.2), $\langle \phi \mid \chi_+^{(0)}(t) \rangle$ can be put in the following form:[12]

$$\langle \phi \mid \chi_+^{(0)}(t) \rangle$$
$$= W(\phi, t) \exp\left[-i\left[\frac{\hbar \omega_0^2}{4\Omega N_0^2} + \tfrac{1}{4}\alpha N_0^2 \hbar \Omega + s\right] t / \hbar\right] \ , \tag{3.6}$$

where

$$W(\phi, t) = \exp\left[\frac{i\omega_0 \phi}{2\Omega N_0}\right] U_\alpha[\tfrac{1}{2}(N_0 \phi - \omega_0 t)] \exp(ist / \hbar) \tag{3.7}$$

and s is some arbitrary constant. The presence of the parameter s is necessary in order to exhaust all the possibilities. Equation (3.5) is satisfied for quasienergy

$$\varepsilon = \frac{\hbar\omega_0^2}{4\Omega N_0^2} + \tfrac{1}{4}\alpha N_0^2 \hbar\Omega + s \ . \tag{3.8}$$

Imposing the condition, Eq. (3.7), the solution to the Mathieu equation, U_α, must be of the form of a Floquet solution:[17]

$$U_\alpha(\phi,t) = e^{iv\theta} Q(\theta), \quad Q(\theta) = Q(\theta + \pi) \ , \tag{3.9}$$

where v is the characteristic exponent with

$$v = 2s / \hbar\omega_0 \ . \tag{3.10}$$

Since ε is real and α is also real, v must be real. Therefore $U_\alpha(\theta)$ is a stable solution. The periodicity condition $\langle -\pi \,|\, \chi_+^{(0)}(t)\rangle = \langle \pi \,|\, \chi_+^{(0)}(t)\rangle$ must also be imposed. With this additional condition, we obtain the following constraint for the characteristic exponent:

$$v = \frac{1}{N_0}\left[2j - \frac{\omega_0}{\Omega N_0}\right] \quad (j \text{ an integer}) \ . \tag{3.11}$$

For each j there is a corresponding characteristic exponent v_j and therefore a corresponding eigenvalue of the Mathieu equation, α_j.[12,17] The corresponding quasienergy is

$$\varepsilon_j = \tfrac{1}{4}N_0^2\alpha_j\hbar\Omega - \frac{\hbar\omega_0^2}{4\Omega N_0^2} + \frac{j}{N_0}\hbar\omega_0 \ . \tag{3.12}$$

Equation (3.12), however, does not exhaust all the possibilities in ϕ space. If W_j satisfies Eq. (3.5) corresponding to eigenvalue ε_j, then

$$W_{jl}(\phi,t) \equiv W_j(\phi,t)e^{il\omega_0 t} \tag{3.13}$$

is also an eigenstate with eigenvalue

$$\varepsilon_{jl} = \varepsilon_j + l\hbar\omega_0 \tag{3.14}$$

$$= \tfrac{1}{4}N_0^2\alpha_j\hbar\Omega - \frac{\hbar\omega_0^2}{4\Omega N_0^2} + \left[\frac{j}{N_0}+l\right]\hbar\omega_0 \ , \tag{3.15}$$

where l is any integer. Equation (3.15) gives the complete quasienergy spectrum. This proves that the quasienergy spectrum for the single-resonance approximation is discrete. Sets of quasienergy of the form given in Eq. (3.14) have been termed the "photon replica state population" and have been observed experimentally.[18]

The most tightly bound state corresponds to the one with the smallest magnitude in v. In Table I we give some j's and their corresponding v's which are in the neighborhood of the most tightly bound state. For specific computations, we choose ω_0 so as to give rise to a resonant transition between $j=150$ and $j=151$ for the unperturbed levels.

TABLE I. Allowed characteristic exponents for the most tightly bound states based on Eq. (3.11).

N_0	j	v_j
1	149	-3
	150	-1
	151	1
	152	3
3	49	$-\frac{7}{9}$
	50	$-\frac{1}{9}$
	51	$\frac{5}{9}$
	52	$\frac{11}{9}$
5	29	$-\frac{11}{25}$
	30	$-\frac{1}{25}$
	31	$\frac{9}{25}$
	32	$\frac{19}{25}$

IV. THE SPECTRUM

We are interested in the effect of resonance overlap. We must construct a wave function which is dominantly composed of quasienergy states which are responsible for the resonance zones. The quasienergy spectrum is then the Fourier spectrum of the wave function (for $\hbar=1$). Therefore we compute the spectrum numerically by initially populating a single level inside the resonance zone and obtain solutions to Eq. (2.9) over a long period of time. We then compute the discrete Fourier transform of the resulting $\langle \phi=0 \,|\, \chi_+^{(\hbar)}(t)\rangle$. Of course, for our system, we must remember that in order to satisfy the boundary conditions at the walls the corresponding level in the negative action must also be properly populated. Using the condition, Eq. (2.8), the wave function can be put in the following form:

$$\Phi(\phi,t) = \Phi_+(\phi,t) + \Phi_-(\phi,t) \ , \tag{4.1}$$

with

$$\Phi_+(\phi,t) = \sum_{j=1}^{\infty} \frac{e^{ij\phi}}{\sqrt{2\pi}}\langle j;I \,|\, \psi(t)\rangle \ , \tag{4.2}$$

$$\Phi_-(\phi,t) = -\sum_{j=1}^{\infty} \frac{e^{-ij\phi}}{\sqrt{2\pi}}\langle j;I \,|\, \psi(t)\rangle \ . \tag{4.3}$$

Therefore, Φ_+ and Φ_- contain the same Fourier spectrum.

We first numerically integrate Eq. (2.9) for $N_0=1$ with initial condition $\langle 153;I \,|\, \chi_+^{(0)}(0)\rangle = 1$ (the magnitude of normalization factor is unimportant for our purpose) and $\langle j;I \,|\, \chi_+^{(0)}(0)\rangle = 0$ for any other j. The total number of levels used in the difference equations is 100 running from $j=101$ to $j=200$. We choose $\rho=25$ which corresponds to $\lambda \simeq 0.038\,05$. This is the maximum value of ρ at which one can find tabulated characteristic values, α of the Mathieu equation for given characteristic exponents, v,

allowed by Eq. (3.11).[19] We have chosen the time interval between discrete times at which the solutions of the wave function are to be found (time sampling) to be about 0.089 227. We have computed the solutions within the data window from $t=0$ to $t=2923.8$. The error in normalization is checked to be less than 3×10^{-6}.

Figure 1 shows the result of numerical computation, where we plot $R(\omega)$, which is the square of the absolute value of the discrete Fourier transform of the function $\langle 0 | X_+^{(0)}(t) \rangle$ versus the angular frequency ω.[12] $R(\omega)$ is proportional to the conventional definition of power spectrum. It is interesting to see that the spectrum forms clusters of discrete lines with an average distance of $\omega_0 \simeq 3.7134$ between adjacent clusters. In Fig. 2 we enlarge two of the clusters. We can compare the ω's at the peaks with the predictions based on Eq. (3.15), shown in Table II. They agree to six significant figures. Notice that the rightmost peak in Figs. 2(a) and 2(b) actually contain two peaks. Due to finite resolving power, the error in ω is about ± 0.001. We find that all the predicted figures lie within the error bars of peak locations. The corresponding peaks in the two clusters are all separated by ω_0. Thus we have obtained a complete agreement between the theory and numerical experiment for the cases tested. In this example, we have obtained ten dominating quasienergy states contributing to this particular state.

It is interesting to determine the effect of the $N=3$ zone on this spectrum when one uses the two-resonance approximation. We have proceeded in exactly the same manner as above except that we have integrated Eq. (2.9) with $\hat{n}=2$. The results we obtain are identical to the previous case. (The only difference is that the maximum error in normalization is about 6×10^{-6}.) This is perhaps not surprising. Since the two resonance zones overlap at $\lambda \simeq 7$,[15] at $\lambda \simeq 0.038\,05$, the two zones are far separated.

At higher λ, we have computed the Fourier spectra for λ small enough that no overlap occurs ($\lambda=4$), and for λ above overlap ($\lambda=9,15$), for three different input data windows, $t \in [8.192,2105.344]$, $[2105.344,4202.496]$, and $[8.192,4202.496]$. The interval $[8.192,4202.496]$ corresponds to about 2479 oscillations of the external field. The number of levels used is chosen so that no significant probability is spread to the edges. (For example, for the double-resonance approximation at $\lambda=15$, the total number of levels used is 300 running from $j=-29$ to $j=270$.) Thus errors in normalization are maintained at below 7×10^{-5}. The time interval between successive data points is 0.004 (the time sampling). For the initial conditions, we have populated a single level near the low-j edge of the $N=1$ resonance zone as estimated by the single-resonance approximation, with the same initial condition for the single- and double-resonance approximation.

The spectra with the data window $[8.192,2105.344]$ are shown in Fig. 3. We can see that at these λ's the spectra for the single- and double-resonance cases are now different. The difference escalates as λ is increased. As a comparison, let us consider the spectra for $\lambda=15$. The total number of peaks (the relative maxima) in the range $\omega \in (-80,720)$ for the single-resonance case is 12 223. For the double-resonance case it is 29 921 in the
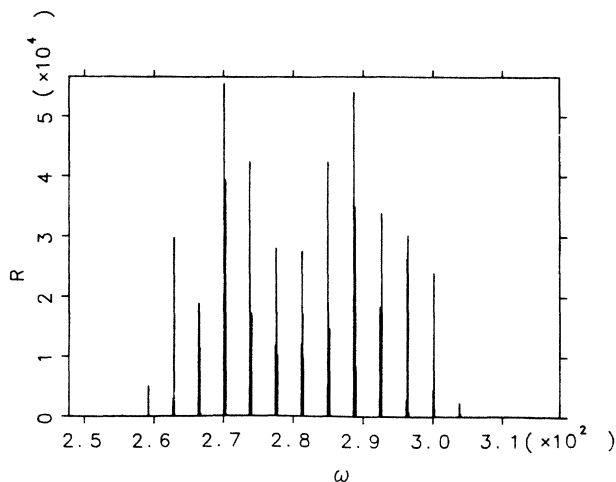
FIG. 1. Absolute square of the discrete Fourier transform of a state initially occupying a single unperturbed level at $j=153$ with $\lambda \approx 0.038\,05$. Identical results are obtained using single- and double-resonance approximations.
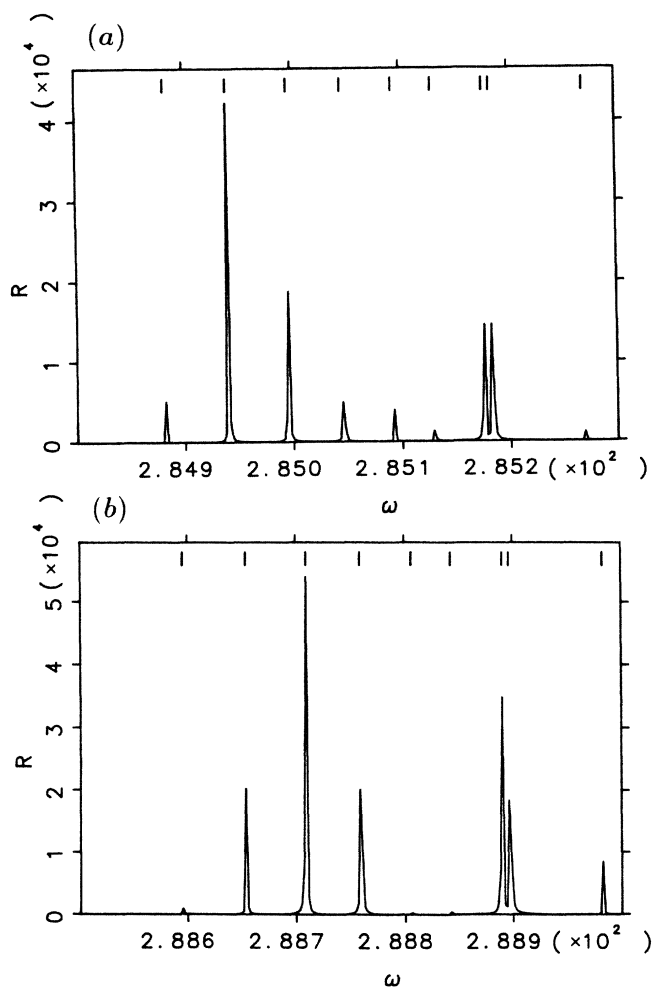
FIG. 2. (a) An enlargement of one of the clusters in Fig. 1. (b) An enlargement of another cluster in Fig. 1. In this figure, as well as Fig. 4, the bars give the locations of the relative maxima.

TABLE II. A comparison of the quasienergy spectrum obtained from theoretical predictions [Eq. (3.15)] with that obtained from numerical experiments (ω) at $\lambda \approx 0.03805$. The numerical results are identical for single- and double-resonance approximations. (a) For the peaks given in Fig. 2(a). (b) For the peaks given in Fig. 2(b).

j	v_j	l	α_j	ε_{jl}	ω
			(a)		
151	1	1	−40.256 778 98	284.882 254 8	284.8823
150	−1	2	−21.314 899 69	284.940 676 3	284.9403
152	3	0	−3.520 941 530	284.995 557 4	284.9961
149	−3	3	12.964 079 44	285.046 401 3	285.0456
153	5	−1	28.062 765 90	285.092 969 5	285.0929
148	−5	4	40.050 190 99	285.129 941 7	285.1294
154	7	−2	55.002 957 15	285.176 059 8	285.1767
147	−7	5	57.534 689 00	285.183 868 3	285.1831
155	9	−3	85.023 356 50	285.268 650 2	285.2691
146	−9	6	85.076 999 88	285.268 815 7	285.2691
			(b)		
151	1	2	−40.256 778 98	288.595 693 5	288.5957
150	−1	3	−21.314 899 69	288.654 115 0	288.6537
152	3	1	−3.520 941 530	288.708 996 0	288.7096
149	−3	4	12.964 079 44	288.759 840 0	288.7590
153	5	0	28.062 765 90	288.806 408 1	288.8063
148	−5	5	40.050 190 99	288.843 380 4	288.8428
154	7	−1	55.002 957 15	288.889 498 4	288.8901
147	−7	6	57.534 689 00	288.897 306 9	288.8965
155	9	−2	85.023 356 50	288.982 088 9	288.9825
146	−9	7	85.076 999 88	288.982 254 4	288.9825

same range. This indicates that the addition of the $N = 3$ term has the effect of increasing the degree of aperiodicity. In Fig. 4 we enlarge the spectra in a small section for $\lambda = 15$. They show that the quasienergy spectrum is discrete, to within numerical accuracy. We will compute spacing distributions for the spectra for $\lambda = 4, 9, 15$ and then compare them with a theoretical distribution to measure the degree of spectral repulsion.

V. THE DISTRIBUTION OF NEAREST-NEIGHBOR SPACINGS

The spacings considered are simply those between peaks in the spectrum. Due to the finite length of the data window, there exists a minimum spacing S_c that one can observe in the Fourier spectrum. To make an accurate comparison of the observed distribution with a theoretical distribution, one must somehow take into account this factor.[2,12]

Consider a theoretical distribution $P(S)$, $S \in [0, \infty)$. $P(S)dS$ gives the probability for observing a spacing in the range $[S, S+dS]$, and $\int_0^\infty P(S)dS = 1$. We will compare the theoretical distribution with the experimental unfolded spectra. For the unfolded spectrum, the local average spacing is constant throughout the entire spectrum and is equal to the average spacing over the entire spectrum. If experiments (real or numerical) cannot detect anything below S_c, it is necessary to construct a truncated distribution,

$$P'(S) \equiv \frac{P(S)}{\int_{S_c}^\infty P(S)dS}, \quad S \in [S_c, \infty) . \tag{5.1}$$

Obviously,

$$\int_{S_c}^\infty P'(S)dS = 1 , \tag{5.2}$$

$$\int_{S_c}^\infty SP'(S)dS = D' , \tag{5.3}$$

where D' is the average spacing over the range $[S_c, \infty)$. We also have

$$\int_{S_c}^\infty P(S)dS = N_1'/N_1 , \tag{5.4}$$

where N_1 (N_1') is the total number of spacings in the range $(0, \infty)$ ($[S_c, \infty)$). To express the distribution in units of the local average spacing, we make a change of variable $y = S/D'$. The distribution in y is then

$$P'(y) = \frac{N_1}{N_1'} D'P(S) \mid_{S=D'y}, \quad y \in [y_c, \infty) \tag{5.5}$$

where $y_c = S_c/D'$. $P'(y)$ has the following property:

$$\int_{y_c}^\infty P'(y)dy = \int_{y_c}^\infty yP'(y)dy = 1 . \tag{5.6}$$

In our subsequent analysis we will use[20] the Brody dis-
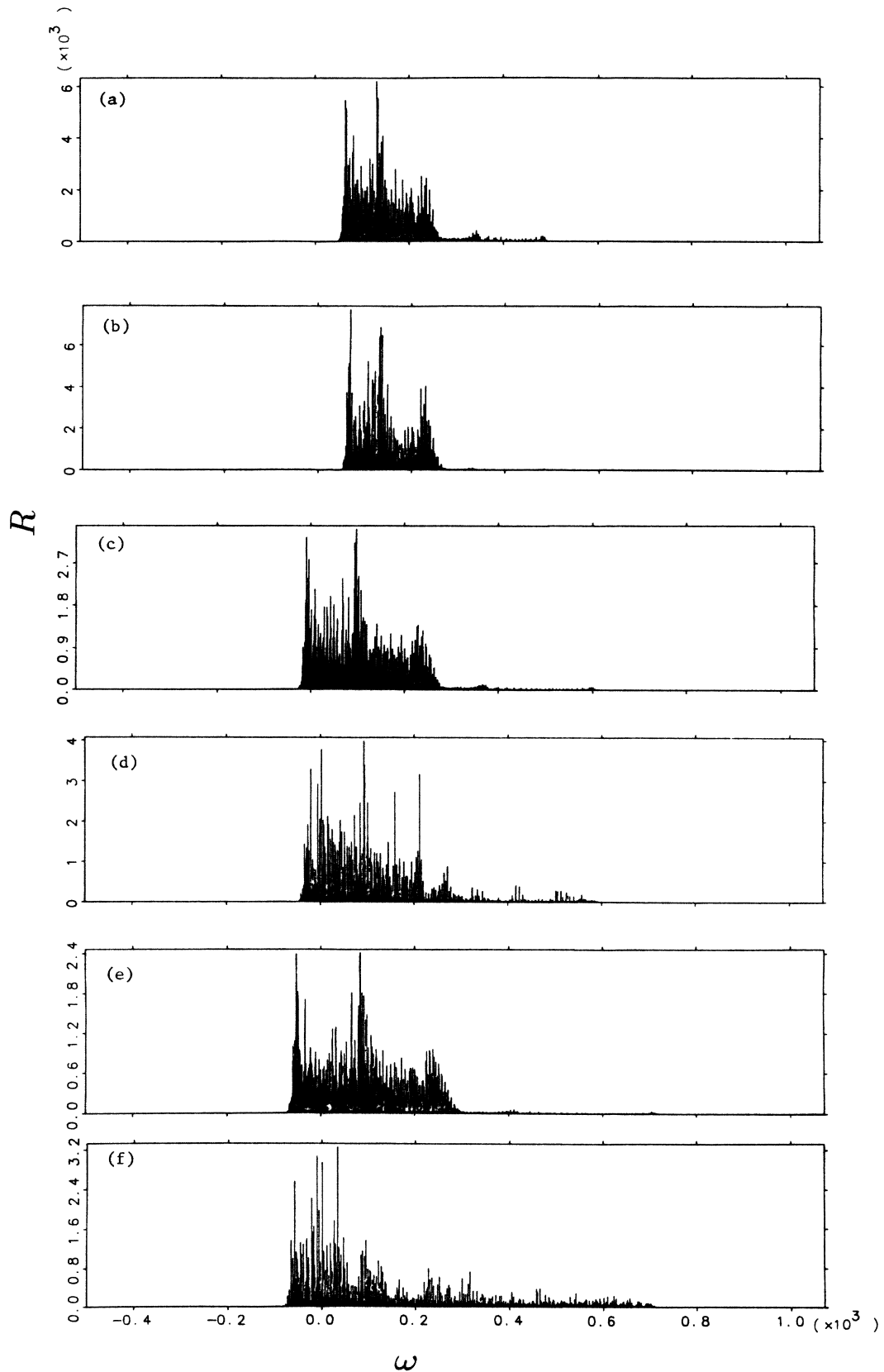
FIG. 3. Absolute square of the discrete Fourier transform of a state initially occupying a single unperturbed level at the low-j edge of $N=1$ resonance zone with the data window [8.192,2105.344] using (a) single-resonance approximation at $\lambda=4$, (b) double-resonance approximation at $\lambda=4$, (c) single-resonance approximation at $\lambda=9$, (d) double-resonance approximation at $\lambda=9$, (e) single-resonance approximation at $\lambda=15$, (f) double-resonance approximation at $\lambda=15$.

tribution $P_q(S)$, which is defined as[21]

$$P_q(S) = (1+q)\beta S^q \exp(-\beta S^{1+q}) ,$$

$$\beta = \left[\frac{1}{D} \Gamma \left(\frac{2+q}{1+q} \right) \right]^{1+q} , \qquad (5.7)$$

where D is the local average spacing. It becomes a Poisson distribution for $q = 0$ and a Wigner distribution for $q = 1$. Thus the Brody parameter q measures the degree of spectral repulsion.[5] Using Eqs. (5.4) and (5.5), we obtain the following truncated Brody distribution:

$$P_q'(y) = A^{1+q}(1+q)B(q)y^q$$

$$\times \exp[-A^{1+q}B(q)(y_c^{1+q} - y^{1+q})] , \qquad (5.8)$$

where $A = D'/D$, $B(q) = (\Gamma[(2+q)/(1+q)])^{1+q}$ and $y \in [y_c, \infty]$. It is important to note that for $q = 0$ and $q = 1$ the distribution $P_q'(y)$ has a qualitatively different dependence on y. Thus even moderate values of y give significant information on the value of q.

The peak locations in our Fourier spectra are at the relative maxima of $R(\omega)$. There exist possibilities that
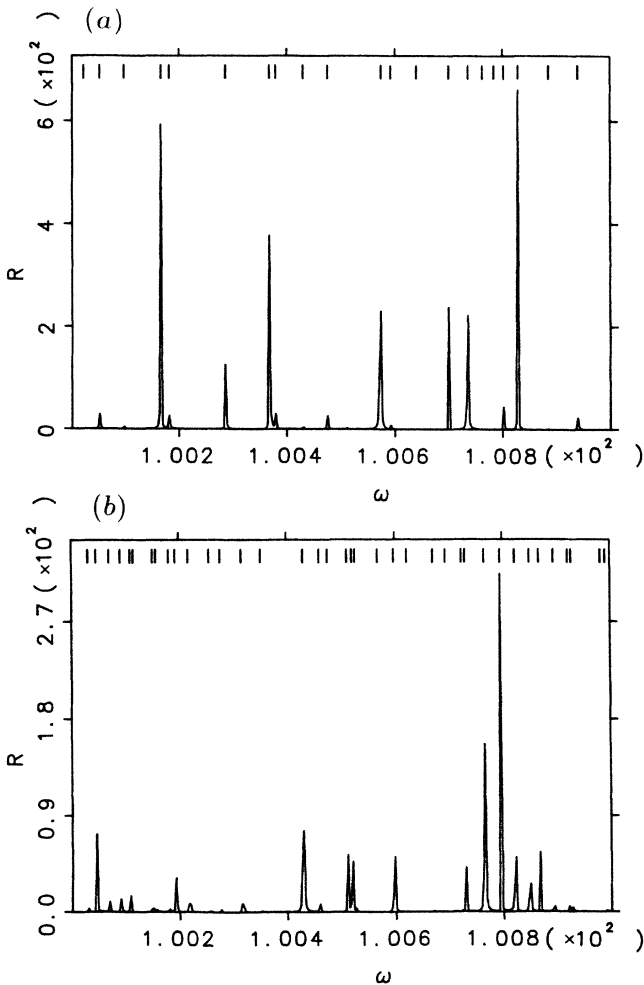
the relative maxima do not correspond to true peaks due to the nature of discrete Fourier transform. We have analyzed this problem and have shown[12] that this probability is very small as long as one concentrates on the region with strong power spectrum, and is unlikely to alter the overall statistics significantly. In fact, for $\lambda = 0.03805$, we found no maxima which were inconsistent with our prediction, Eq. (3.15).

At the edges of strong power spectra the level densities decrease sharply. So we have eliminated the edges to obtain "good spectra"[8] for computing statistics. The spectral ranges covered are $\omega \in [115,450]$ for $\lambda = 4$, $\omega \in [60,540]$ for $\lambda = 9$, and $\omega \in [0,650]$ for $\lambda = 15$, for both single- and double-resonance approximations. The good spectra are then unfolded by fitting the staircase function $F(\omega) = \sum_i \Theta(\omega - \omega_i)$, where Θ is the Heaviside step function, with least-squares cubic splines to remove the secular behavior.[3,5] Figure 5 gives the staircase functions with the splines superimposed for the cases with $\lambda = 15$.

Because of the secular variations, identical spacings in the original spectrum generally become different after unfolding due to their different locations in the original spectrum. This spread in the unfolded spectrum is given by $y_{l,\max} - y_{i,\min} = S_i/D_{\min}' - S_i/D_{\max}'$, where S_i $(i = 1, 2, \ldots)$ is a given spacing with S_1 being the minimum spacing observed and $D_{\max}'$ and $D_{\min}'$ are maximum and minimum of local average spacing in the original spectrum (before unfolding). We see that the spread increases linearly with S_i. Figure 6 gives a schematic representation of this mapping. The dashed arrows correspond to the mappings if spacings S_0, S_{-1} were observed (by increased resolving power). From the figure, we see that there are fewer spacings mapped into the interval $[y_{1,\min}, y_{1,\max}]$ than if we had better resolving power. Thus the distribution below $y_{1,\max}$ cannot be obtained accurately. Consequently, we will neglect any spacing smaller than $y_{1,\max}$ and compute the truncated distributions with $y_c = y_{1,\max}$. Since the frequency grid for a finite data window T is $2\pi/T$, the minimum spacing one can observe in the spectrum is $S_1 = 4\pi/T$. So we obtain $y_c = 4\pi/TD_{\min}'$, where $D_{\min}'$ is computed from the splines. Once the truncated distribution beginning from the y_c given above is computed, we measure its spectral repulsion. This is performed with a nonlinear least-squares best fit of Eq. (5.8) to the observed distribution, which minimizes the sum of the square of the differences between the total probability observed in each bin and that computed from Eq. (5.8). The best-fit parameters q and A are thus found.

Figures 7–9 present the results. From Figs. 7 and 8 we can see that, with T being the same, the distributions are insensitive to the initial time of the data window. For the single-resonance approximation, the distributions are close to the Poisson type for all λ's (the q for $\lambda = 4$ is slightly large; this appears to be due to the smaller number of spacings involved and the resulting poorer statistics). This is consistent with our expectation, since the single-resonance approximation is integrable. For the double-resonance approximation, the distribution is close

FIG. 4. (a) An enlargement of a small section in Fig. 3(e). (b) An enlargement of a small section in Fig. 3(f).
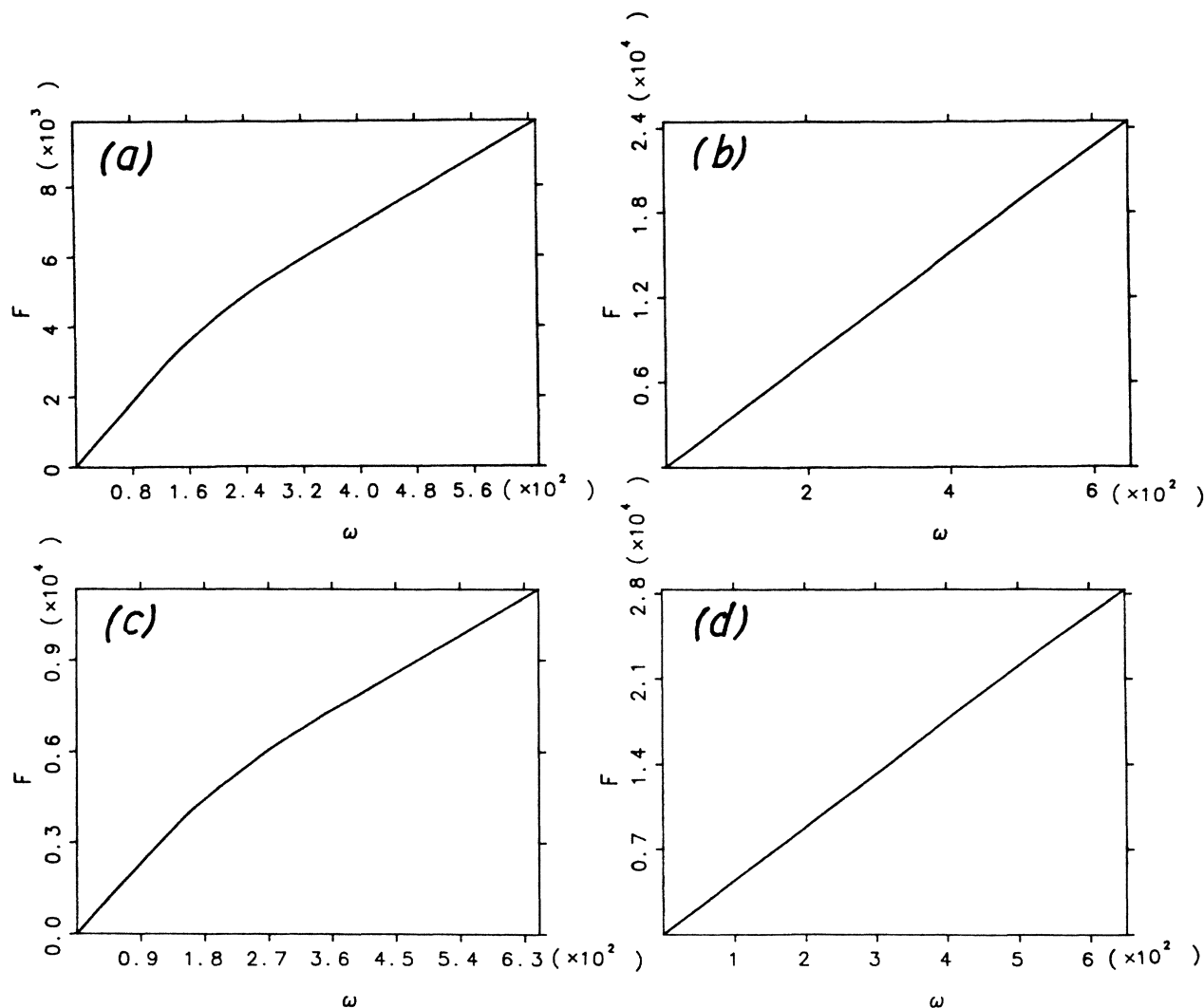
FIG. 5. Staircase functions of the spectrum with the least-squares cubic splines superimposed for (a) single-resonance approximation at $\lambda=15$ with the data window [8.192,2105.344], (b) double-resonance approximation at $\lambda=15$ with the data window [8.192,2105.344], (c) single-resonance approximation at $\lambda=15$ with the data window [8.192,4202.496], (d) double-resonance approximation at $\lambda=15$ with the data window [8.192,4202.496].

to Poisson type at $\lambda=4$, although with quite a bit of fluctuations possibly due to the smaller number of spacings involved. As λ is increased to 9 and 15, the distributions are strongly deviated from the Poisson type and tend toward the Wigner type with large spectral repulsions.
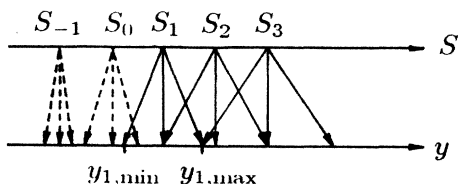
FIG. 6. A Schematic representation of the unfolding procedure showing that, at the edge of the small spacing in the unfolded spectrum, there are generally fewer spacings than it should have if there were infinite resolving power.

Thus the spectrum in the region of the resonance zones undergoes a change in its characteristic from a predominantly mixed sequence to a predominantly pure sequence through resonance overlap. For the longer data window as presented in Fig. 9, the Brody parameter decreases for the double-resonance approximation at $\lambda=9$ and 15. This appears to occur because for the initial condition chosen, the wave function is composed not only of quasienergy states responsible for the resonance zones but also of those which are responsible for the nonresonant region although with much smaller amplitudes. When the length of data window is increased, one is seeing more contributions coming from the nonresonant regions because of the reduction in leakage in the discrete Fourier transform. But still, the repulsion in the spectrum is non-negligible. Also notice that for $\lambda=15$ the best-fit truncated Brody distribution actually does not fit quite well. Apart from the first bin the spectrum appears to have more repulsion than measured.

VI. THE Δ_3 STATISTIC

The Δ_3 statistic gives a measure of departure from long-range spectral rigidity. It is defined as[8]

$$\Delta_3(n,\omega') = \frac{1}{n\bar{D}} \min_{A_1, A_2} \int_{\omega'}^{\omega'+n\bar{D}} [F(\omega) - A_1\omega - A_2]^2 d\omega .$$

(6.1)

The interval $[\omega',\omega'+n\bar{D}]$ contains n spacings, $\bar{D}$ is the average spacing over the interval, and $F(\omega)$ is the staircase function of an unfolded spectrum. A_1 and A_2 are to be chosen to minimize the integral.

We have computed the spectral averaged Δ_3 statistic.[6] If we denote the whole sequence of an unfolded spectrum by $\omega_1,\omega_2, \ldots ,\omega_{k-1},\omega_k$ in ascending order, where k is
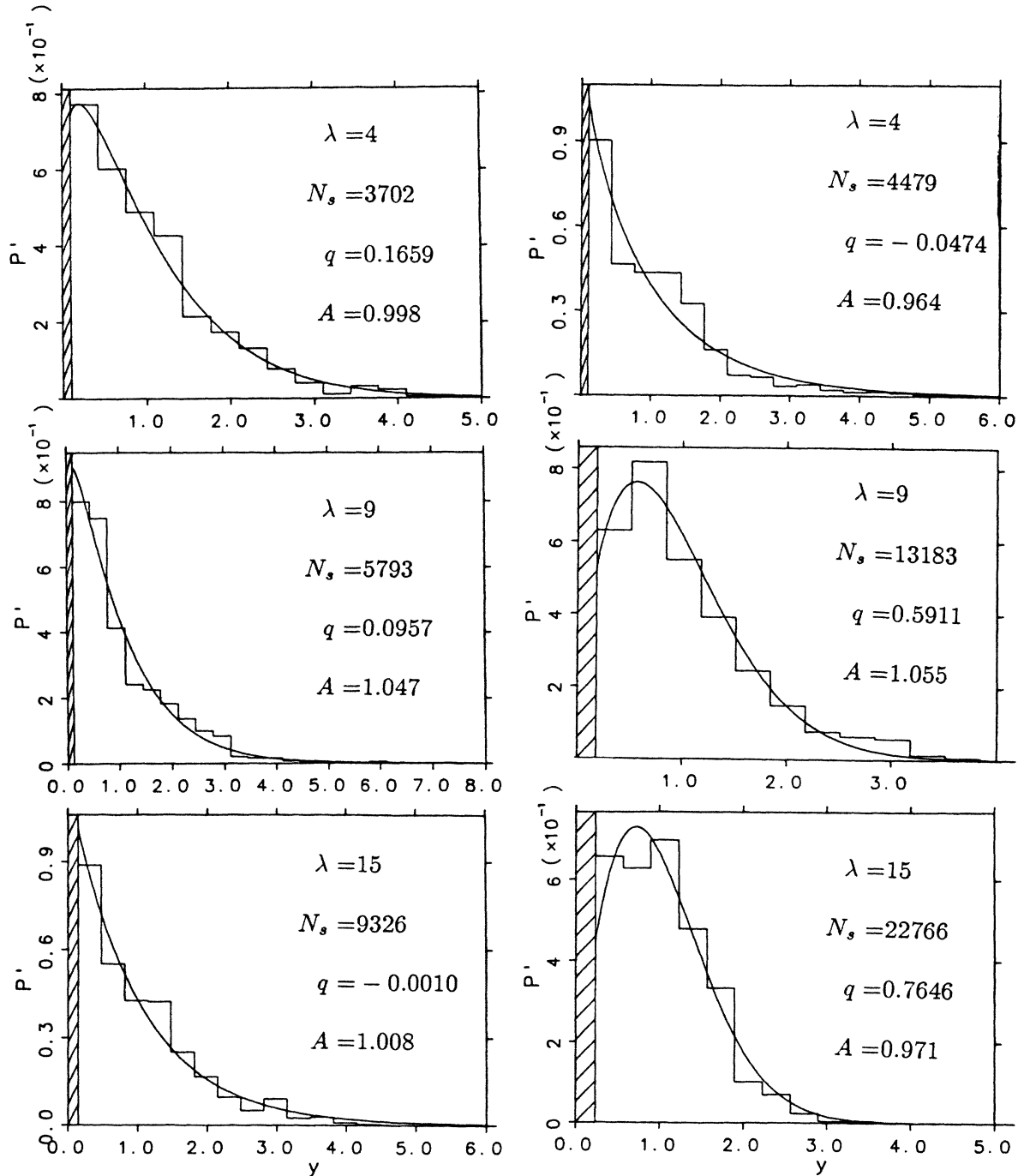
FIG. 7. Spacing distributions from numerical experiments (curve of steps) and its best-fit truncated Brody distributions (smooth curve) for the data window [8.192,2105.344]. The slashed part corresponds to the unobserved region $[0,y_c)$. N_s is the total number of spacings involved in the experimental distribution. The left column is for single-resonance approximation and the right column is for the double-resonance approximation.

the total number of peaks, the spectral averaged Δ_3 statistic is given by

$$\overline{\Delta}_3(n) \equiv \frac{1}{k-n-1} \sum_{i=1}^{k-n-1} \Delta_3(n,\omega_i')$$

$$\text{with } \omega_i' = \tfrac{1}{2}(\omega_i + \omega_{i+1}) \ .$$

The interval over which $\Delta_3(n,\omega_i')$ is computed is

$$\omega \in [\omega_i',\omega_i''] \quad \text{with } \omega_i'' = \tfrac{1}{2}(\omega_{i+n} + \omega_{i+n+1}) \ .$$

The results for the data window [2105.344,4202.496] are shown in Fig. 10. First we notice that the gap between the single- and double-resonance cases widens as λ is increased. For the double-resonance cases, the Δ_3 statistic approaches the GOE results as λ is increased. This is a further confirmation of the strong effect of quantum-resonance overlap. For the single-resonance cases, the Δ_3 statistic is lower than the case with totally uncorrelated spacings. The presence of this long-range correlation for an integrable system has been observed in
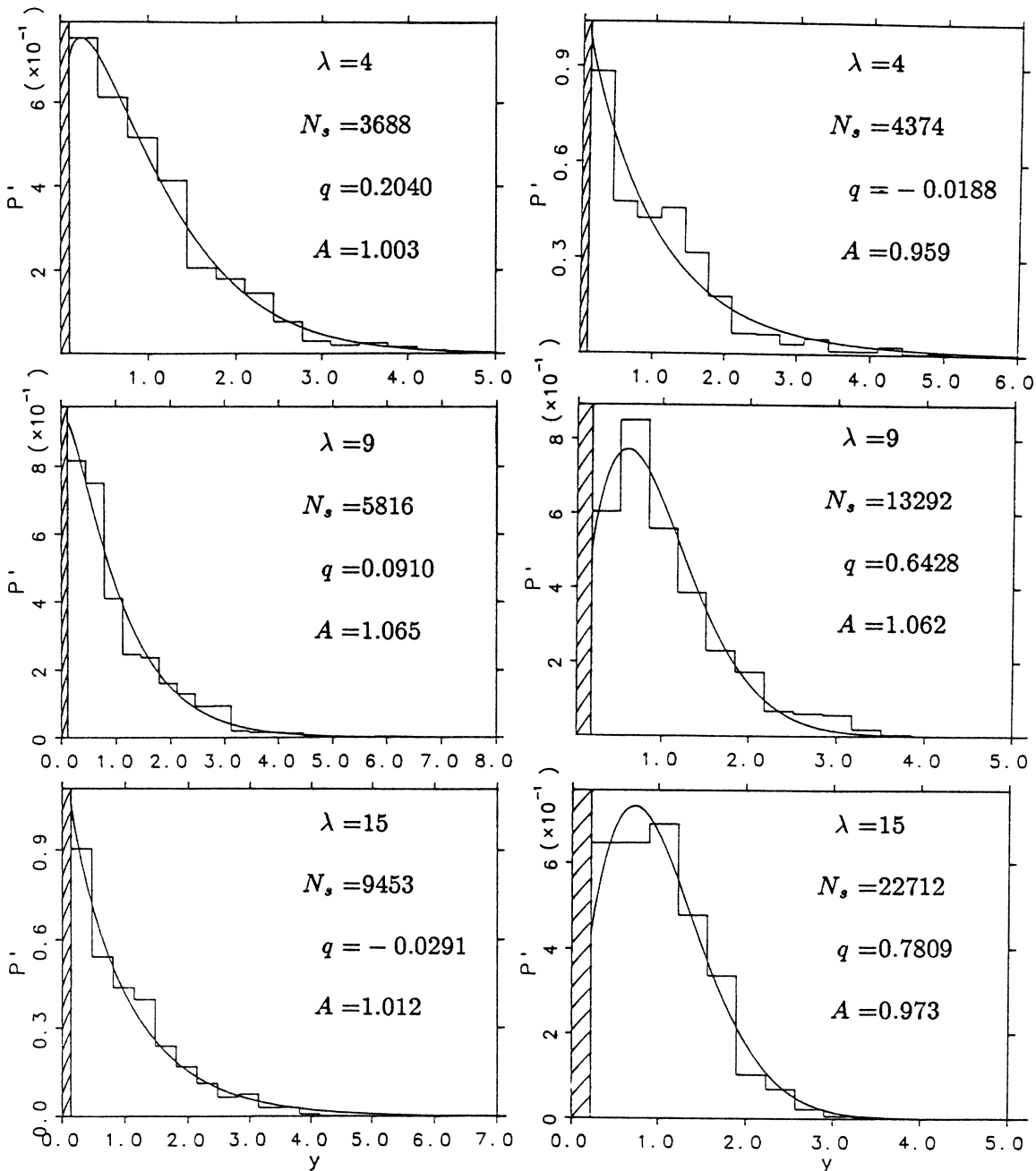
FIG. 8. Same as Fig. 7 but for the data window [2105.344,4202.496].

several studies,[22] where it was found that the Δ_3 statistic eventually saturates as n is increased. In the present case, the saturation effect appears to be forced by photon replica so that the spectrum must more or less repeat itself over an interval ω_0. Since, in our data, the number of spacings in this interval increases as λ is increased, it sat-

urates at larger n for higher λ. This explains what we have observed. Of course, the computations are subject to the errors due to the unobserved small spacings because of finite resolving power. But by extrapolations of Fig. 8, the proportions of unobserved spacings are small, and, therefore, should only have small effects.
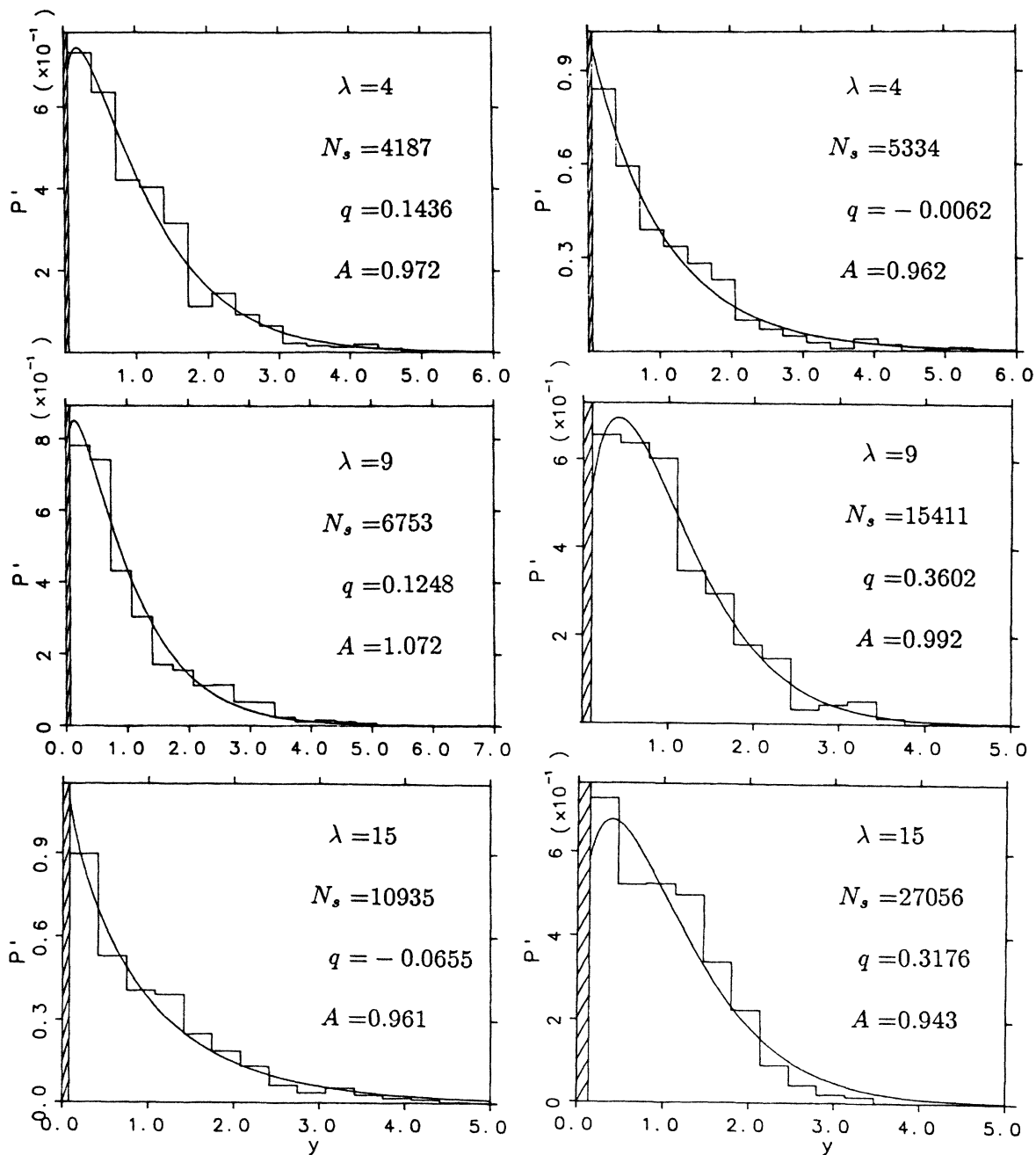
FIG. 9. Same as Fig. 7 but for the data window [8.192,4202.496].
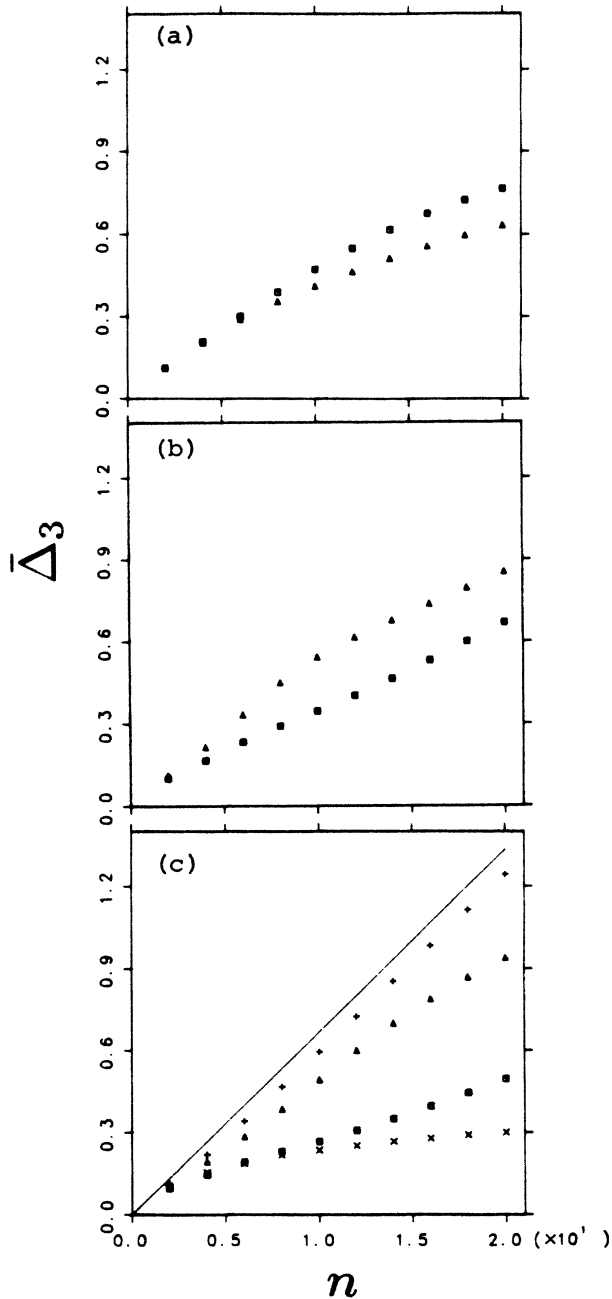
FIG. 10. Spectral averaged Δ_3 statistic for the data window [2105.344,4202.496]. The triangular markers correspond to the single-resonance case. The square markers correspond to the double-resonance case. (a) $\lambda=4$, (b) $\lambda=9$, (c) $\lambda=15$. In (c), the $\times$ markers correspond to the GOE result of Ref. 6, the $+$ markers correspond to the spectrum obtained by ordering 10000 numbers generated by the random number generator, and the straight line is $n/15$, expected for a spectrum with totally uncorrelated spacings.

VII. DISCUSSIONS AND CONCLUSION

In summary, for the single-resonance Hamiltonian, we have derived a formula which relates the quasienergy spectrum to the eigenvalues of the Mathieu equation. This formula and the subsequent numerical verification have helped us to understand the resonance zone as being composed of states of the particle trapped in the traveling cosine potential well. The quasienergy spacing distributions computed are close to the Poisson distribution. The closeness gets better as the number of spacing involved is increased when λ is increased. This is a confirmation of Mehta's theorem since from the outset we know that the spectrum is a mixed sequence.

For the double-resonance Hamiltonian, the quasienergy spectrum is found to be identical to that for the single-resonance Hamiltonian at very small λ ($\lambda=0.03805$). This provides a check for the validity of single-resonance approximation at small λ. It is also a quantum manifestation of the KAM theorem[23] in the sense that the system behaves like an integrable system at small-enough perturbations. There appear to be two constants of motion. One is global and the other is local. Classically, the existence of a local constant of motion forms the basis of KAM theorem. We have here seen the manifestation of this phenomenon in a microscopic quantum domain. At larger λ ($\lambda=4$) but below resonance overlap, the spacing distribution is close to Poisson. Since it is not clear if the converse of Mehta's theorem is true, observing a Poisson distribution itself does not guarantee that the spectrum is a mixed sequence. But the fact that the Hamiltonian is close to an integrable one for sufficiently small λ's, together with the fact that, to our best knowledge, no known pure sequence exhibits Poisson distribution, strongly indicate that it is a predominantly mixed sequence. This means that for the majority of the quasienergy levels involved they can be labeled by two quantum numbers and consequently the preservation of the local constant of motion. At larger perturbations when the resonance zones overlap, we have found strong deviations from Poisson distribution toward GOE distribution. One can argue that the reason we do not see Poisson distribution is because too few spacings are involved. But the fact the we have presented many Poissonian distributions with far less spacings shows that this is not the case. Thus what we have observed are predominantly pure sequences. It signifies the destruction of the local constant of motion and its corresponding quantum number through quantum-resonance overlap. This is a quantum manifestation of classical-resonance overlap where the destruction of all the nonresonant tori between the two resonance zones implies the destruction of the local constant of motion in a large part of phase space. The computations of Δ_3 statistic further confirm such a picture.

[1]M. V. Berry and M. Tabor, Proc. R. Soc. London, Ser. A **356**, 375 (1977); M. V. Berry, in *Chaotic Behavior of Deterministic Systems*, Proceedings of the Les Houches Summer School, edited by G. Iooss, R. H. G. Helleman, and R. Stora (North-Holland, Amsterdam, 1981); P. Pechukas, Phys. Rev. Lett. **51**, 943 (1983); O. Bohigas, M. J. Giannoni, and C. Schmit, *ibid.* **52**, 1 (1984); T. H. Seligman, J. J. M. Verbaarschot, and M. R. Zirnbauer, *ibid.* **53**, 215 (1984); G. Casati, B. V. Chirikov, and I. Guarneri, *ibid.* **54**, 1350 (1985); F. M. Israilev, *ibid.* **56**, 541 (1986); J. V. José and R. Cordery, *ibid.* **56**, 290 (1986).

[2]E. Abramson, R. W. Field, D. Imre, K. K. Innes, and J. L. Kinsey, J. Chem. Phys. **80**, 2298 (1984).

[3]E. Haller, H. Köppel, and L. S. Cederbaum, Phys. Rev. Lett. **52**, 1665 (1984).

[4]T. Terasaka and T. Matsushita, Phys. Rev. A **32**, 538 (1985).

[5]T. A. Brody, J. Flores, J. B. French, P. A. Mello, A. Pandey, and S. S. M. Wong, Rev. Mod. Phys. **53**, 385 (1981).

[6]R. U. Haq, A. Pandey, and O. Bohigas, Phys. Rev. Lett. **48**, 1086 (1982).

[7]M. L. Mehta, *Random Matrices and the Statistical Theory of Energy Levels* (Academic, New York, 1967).

[8]F. J. Dyson and M. L. Mehta, J. Math. Phys. **4**, 701 (1963).

[9]Ya. B. Zel'dovich, Zh. Eksp. Teor. Fiz. **51**, 1492 (1966) [Sov. Phys.—JETP **24**, 1006 (1967)]; Usp. Fiz. Nauk **110**, 139 (1973) [Sov. Phys.—Usp. **16**, 427 (1973)].

[10]H. Sambe, Phys. Rev. A **7**, 2203 (1973).

[11]A. J. Lichtenberg and M. A. Lieberman, *Regular and Stochastic Motion* (Springer-Verlag, New York, 1983).

[12]W. A. Lin, dissertation, University of Texas at Austin, 1986 (unpublished).

[13]B. V. Chirikov, Phys. Rep. **52**, 263 (1979).

[14]G. P. Berman and G. M. Zaslavskii, Phys. Lett. **61A**, 295 (1977); G. P. Berman, G. M. Zaslavskii, and A. R. Kolovsky, *ibid.* **87A**, 152 (1982); G. P. Berman and A. R. Kolovsky, *ibid.* **95A**, 15 (1983); G. P. Berman, G. M. Zaslavskii, and A. R. Kolovsky, Zh. Eksp. Teor. Fiz. **81**, 506 (1981) [Sov. Phys.—JETP **54**, 272 (1981)].

[15]L. E. Reichl and W. A. Lin, Phys. Rev. A **33**, 3598 (1986).

[16]W. A. Lin and L. E. Reichl, Physica D **19**, 145 (1986).

[17]*Handbook of Mathematical Functions*, edited by M. Abramowitz and I. A. Stegun (Dover, New York, 1970).

[18]J. E. Bayfield, Phys. Rep. **51**, 317 (1979).

[19]*Tables Relating to Mathieu Functions* (Columbia University Press, New York, 1951).

[20]The semiclassical formula of Berry and Robnik [J. Phys. A **17**, 2413, (1984)] does not apply in what we are considering since our potential (see Appendix A.4 in Ref. 12) does not have scaling behavior, the system is in a full quantum regime, and the spectra cover wide ranges.

[21]T. A. Brody, Lett. Nuovo Cimento **7**, 482 (1973).

[22]G. Casati, B. V. Chirikov, and I. Guarneri, Phys. Rev. Lett. **54**, 1350 (1985); Th. Zimmermann, H.-D. Meyer, H. Köppel, and L. S. Cederbaum, Phys. Rev. A **33**, 4334 (1986); T. H. Seligman and J. J. M. Verbaarschot (unpublished).

[23]G. Hose and H. S. Taylor, Phys. Rev. Lett. **51**, 947 (1983); L. E. Reichl and W. A. Lin, Found. Phys. **17**, 689 (1987).